SCIENCE CHINA
Physics, Mechanics & Astronomy

• Article •

December 2025 Vol. 68 No. 12: 126111
https://doi.org/10.1007/s11433-025-2775-1

Ultrafast surface diffusion driven by abnormal relaxation mode in the marginal glass-forming Fe-based metallic glasses

Yebei Wang[1,2†], Yunhe Gao[1†], Jiajie Lv[1,2], Meichen Jian[1], Yue Huang[1], Yan Li[1], Wenlin Liu[1,2], Yu Tong[1], Yan Zhang[1], Yanping Wei[1], Xiao Jin[1*], Juntao Huo[1*], Junqiang Wang[1*], and Meng Gao[1*]

[1] *Ningbo Institute of Materials Technology & Engineering, Chinese Academy of Sciences, Ningbo 315201, China*
[2] *Center of Materials Science and Optoelectronics Engineering, University of Chinese Academy of Sciences, Beijing 100049, China*

Received April 28, 2025; accepted August 11, 2025; published online September 29, 2025

Atomic surface mobility of glasses plays an important role in understanding glass dynamics and determining many fundamental processes on the surface. However, the diffusion dynamics at the free surface in marginal glasses remains unknown due to limited glass formation ability. In this study, we systematically investigate surface diffusion and relaxation behavior in four marginal glass-forming Fe-based metallic glasses with great application potential. Surface diffusion rates in marginal glass-forming Fe-based metallic glasses are significantly faster than those of stable metallic glasses. For the first time, an abnormal β_t relaxation mode with thermal activation character is identified between α and β relaxation. Strikingly, the activation energy of surface diffusion matches that of β_t relaxation. A mechanism involving cooperative cluster motion associated with β_t relaxation is proposed to explain the ultrafast surface diffusion. These results establish a direct correlation between surface diffusion and bulk relaxation, providing a basis for tailoring surface properties in metallic glasses.

surface diffusion, relaxation, dynamic mechanical analysis, collective cluster motion, metallic glass

PACS number(s): 36.40.Sx, 62.40.+i, 68.35.Fx, 68.37.Ps, 81.05.Kf

Citation: Y. Wang, Y. Gao, J. Lv, M. Jian, Y. Huang, Y. Li, W. Liu, Y. Tong, Y. Zhang, Y. Wei, X. Jin, J. Huo, J. Wang, and M. Gao, Ultrafast surface diffusion driven by abnormal relaxation mode in the marginal glass-forming Fe-based metallic glasses, Sci. China-Phys. Mech. Astron. **68**, 126111 (2025), https://doi.org/10.1007/s11433-025-2775-1

1 Introduction

Metallic glasses (MGs) have attracted extensive attention owing to their outstanding physical and chemical properties [1-4]. Among various MGs, Fe-based MGs are a unique and crucial family distinguished by their superior yield strength, high thermal stability, remarkable corrosion resistance, and excellent soft magnetic properties. It makes Fe-based MGs widely applied in various new material fields, such as soft magnetic applications, wear-resistant and corrosion-resistant coatings, biomedical materials, precision gear micro-motors, fine and precise polishing media, and catalysts [5-7]. The related studies have become the focus of academic and industrial research in the area of MGs. Especially in the high-frequency and high-power electronics field, Fe-based MGs and their nanocrystalline derivatives with high magnetic permeability and low coercivity exhibit exceptional advantages compared to other soft magnetic materials [8-10]. Nevertheless, the electromagnetic field distribution becomes surface-dominated due to the skin effect at extremely high

†Equally contributed to this work.
*Corresponding authors (Meng Gao, email: gaomeng@nimte.ac.cn; Juntao Huo, email: huojuntao@nimte.ac.cn; Junqiang Wang, email: jqwang@nimte.ac.cn; Jin Xiao, email: jinxiao@nimte.ac.cn)

frequencies [11-13], leading to increased energy loss. Thus, the challenges that Fe-based MGs encounter in the high-frequency applications are closely related to the surface dynamics [14,15]. Meanwhile, considering that most Fe-based MGs are marginal glass-formers with limited glass-forming ability, requiring extremely high cooling rates to avoid crystallization, their inherent surface crystallization tendency is also linked to surface dynamics [16-18]. Consequently, understanding the surface dynamics of Fe-based MGs is crucial for soft magnetic applications. Despite the critical need, the surface dynamics of Fe-based MGs remains largely unexplored due to their marginal glass-forming nature.

Understanding the structure-dynamics correlation remains a fundamental goal in glassy materials research. Notable advances in bulk dynamics of MGs contrast with the uncharted structural-dynamical mechanisms governing their surface regions [19-21]. Surface dynamics, especially for the surface diffusion, underpin numerous physical processes, including surface dissipation, surface crystallization, surface failure, and the fabrication of ultrastable glasses [22-26]. Extensive research has demonstrated that surface diffusion in various glasses exceeds their bulk counterparts by 3-5 orders of magnitude [27-35]. The fast surface dynamics may lead to a different microstructure between the surface and the interior of MGs, giving rise to a spectrum of surface-dictated functionalities ranging from enhanced catalytic activity to tunable tribological performance. From this perspective, the discovery of significantly enhanced surface diffusion dynamics in glass materials stands as one of the most impactful theoretical developments in condensed matter physics over recent decades. Moreover, the universal enhancement of surface diffusion exhibits a strong correlation with bulk fragility [32]. On the one hand, Considering the established correlation between bulk fragility and relaxation dynamics [35,36], surface diffusion dynamics can be effectively tuned through manipulation of bulk relaxations. On the other hand, in contrast to stable MGs, several studies have reported that there exist more complex and unexpected relaxation patterns in marginal glass-forming Al- and LaGa-based MGs [37-39]. However, for these marginal glass-forming MGs, the influence of complex relaxations on surface diffusion dynamics remains an open question. Recently, the experimental strategy based on the annealing-induced decay of surface gratings and scratches has been successfully used to determine the surface diffusion dynamics in various glass materials [29-32]. Therefore, this strategy provides a good opportunity to detect the unknown surface diffusion dynamics in marginal glass-forming glasses.

In this work, by taking one typical marginal glass-forming Fe-based MG system (FINEMET) with significant application potential as the model material, we systematically investigated the surface diffusion dynamics and corresponding relaxation characteristics by combining annealing-induced decay of surface scratches with dynamic mechanical analysis. It was found that the surface diffusion rates of these marginal glass-forming Fe-based MGs are significantly faster than those of other stable MGs. By comparing the activation energies of surface diffusion and various bulk relaxation modes, we revealed that the ultrafast surface diffusion is determined by an abnormal relaxation mode related to the cooperative cluster motion. Finally, one simple scheme was proposed to illustrate the relationship between surface diffusion dynamics and bulk relaxation dynamics in marginal glass-forming MGs.

2 Materials and method

2.1 Material preparation and structural characterization

Master alloy ingots with four nominal compositions of $Fe_{77.5}Si_{13.5}B_9$, $Fe_{76.5}Si_{13.5}B_9Cu_1$, $Fe_{74.5}Si_{13.5}B_9Nb_3$, $Fe_{73.5}Si_{13.5}B_9Cu_1Nb_3$ (at.%) were fabricated by induction melting with the mixture of pure Fe, Si, B, Nb, and Cu under an argon atmosphere. The used metals are 99.9% pure. Subsequently, the homogenized ingots were separately sectioned and cut into smaller pieces. One of these smaller pieces was used to prepare the ribbon samples by single-roller melt spinning method at a tangential speed of 45 m s^{-1}. The dimensions of the obtained ribbons are 2 m × 2 mm × (20-30) μm (length×width×thickness).

The chemical compositions of the prepared ribbons were confirmed by energy-dispersive spectroscopy (EDS, ZEISS, EVO18). The glassy nature of these ribbon samples was verified by X-ray diffraction (Bruker, D8 Advance) and transmission electron microscope (FEI, Tecnai F20). Figures 1(a), S1, and S2 (Supplementary Information) clearly confirm that all prepared and annealed ribbons are amorphous. The thermodynamic properties were measured by a differential scanning calorimeter (NETZSCH, DSC 404F1) at a heating rate of 20 K min^{-1}. The onset temperatures of the primary crystallization T_x are marked by arrows with detailed values (Figure S3). Notably, no distinct glass transition is observed for all Fe-based MGs in this work, a typical characteristic of the marginal glass former. The glass transition temperature T_g was therefore determined through stress relaxation analysis, as shown in Figures S4 and S5. The detailed estimation method was provided in the Supplementary Information. The values of T_g and T_x are included in Table 1.

2.2 Measurement of surface diffusion dynamics

The measurements of surface diffusion dynamics were performed on the atomic force microscope (AFM, Vecco Dimension 3100, Bruker) according to the method of

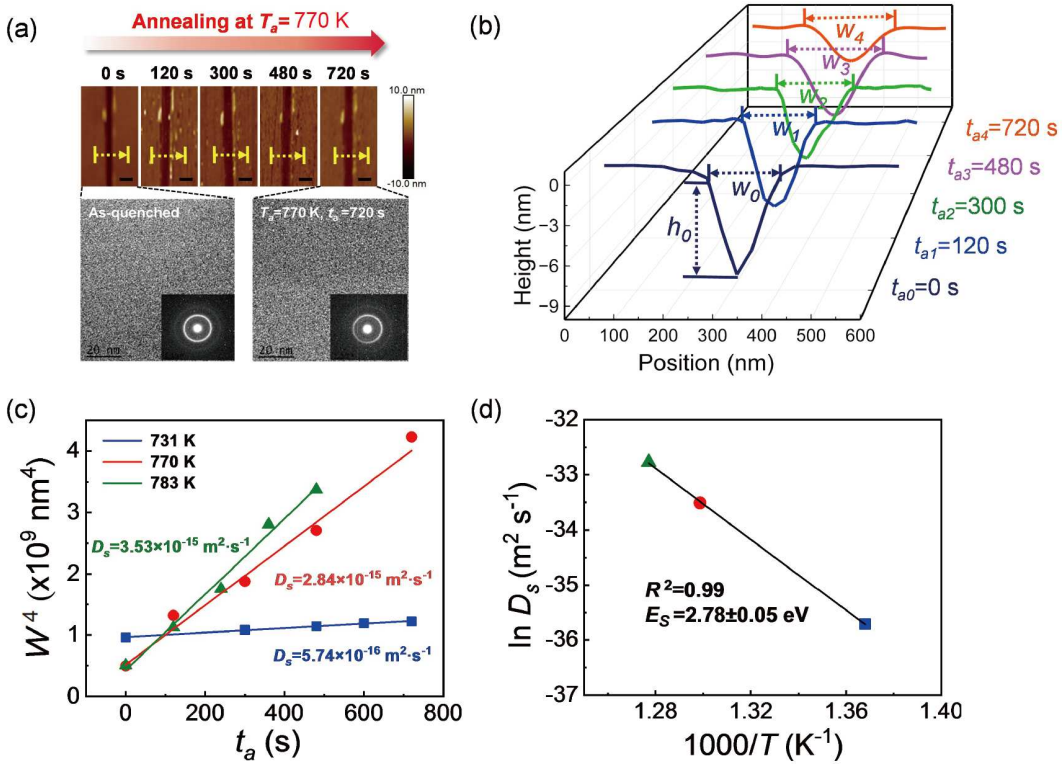

Figure 1 (Color online) Surface diffusion measurements of marginal Fe-based MGs. (a) Atomic force microscope (AFM) images of the evolution of the prepared scratch on the surface of $Fe_{73.5}Si_{13.5}B_9Cu_1Nb_3$ MG at 770 K with different annealing times. The scale bars in AFM images are 250 nm. HRTEM images of as-quenched and annealed samples at 770 K for 720 s are shown below AFM images and the insets show the corresponding selected area electron diffraction patterns (the scale bars are 5 nm^{-1}). (b) Evolution of the cross-sectional morphology of the prepared scratch on the surface of $Fe_{73.5}Si_{13.5}B_9Cu_1Nb_3$ MG along the yellow dashed arrows in Figure 1(a) at 770 K with different annealing times. h_0 and W_0 represent the depth and width of the scratch of the as-cast sample, respectively. W_x represents the width of samples at different annealing times. (c) Scratch width evolution with different annealing times at different temperatures. The experimental data is fitted by eq. (S1) (Supplementary Information) and the corresponding surface diffusion coefficient D_S is included. (d) Plot of the measured D_S and temperature. The solid line represents the best fit according to the Arrhenius equation of $D_S = D_0\exp(-E_S/kT)$.

Table 1 List of glass transition temperature T_g, crystallization temperature T_x, surface diffusion activation energy E_S, β relaxation activation energy E_β, β_t relaxation activation energy $E_{\beta t}$ for marginal Fe-based MGs in this work

Composition	T_g (K)	T_x (K)	E_S (eV)	E_β (eV)	$E_{\beta t}$ (eV)
$Fe_{77.5}Si_{13.5}B_9$	743	783	2.80 ± 0.23	2.16 ± 0.14	2.81 ± 0.09
$Fe_{76.5}Si_{13.5}B_9Cu_1$	703	733	2.35 ± 0.19	1.71 ± 0.09	2.31 ± 0.07
$Fe_{74.5}Si_{13.5}B_9Nb_3$	828	857	2.84 ± 0.17	1.98 ± 0.15	2.78 ± 0.11
$Fe_{73.5}Si_{13.5}B_9Cu_1Nb_3$	768	788	2.78 ± 0.05	2.11 ± 0.04	2.74 ± 0.09

annealing-induced decay of surface scratches [27]. Here, we applied this scratch-smoothing method in view of its advantages compared to other experimental methods. Surface diffusion characterization methods can be categorized into two types: direct detection (e.g., scanning tunneling microscopy (STM), field ion microscopy (FIM)) and indirect detection (e.g., scratch-smoothing, tracing atoms [27,40-43]. However, the methods based on STM and FIM hinder not characterization of collective diffusion behaviors due to the amorphous nature of MGs. For the tracing atoms method, it is challenging to implement the tracing-atoms due to low solubility and diffusion rates in MGs. In contrast, the AFM-based scratch-smoothing approach provides direct, non-destructive measurement of surface diffusion at the nanoscale. What is more, it avoids bulk diffusion interference by restricting scratch depth to < 20 nm, a critical feature for isolating surface dynamics in marginal glass-forming MGs. The applied AFM tips includes: (1) AFM tip for scratch preparing by contact mode: antimony (n) doped Si with a curvature radius of about 30 nm and a force constant of about 200 N m^{-1} (RTESPA-525-30, Bruker); (2) AFM tip for surface topography characterization by tapping mode: phosphorus (n) doped Si with a curvature radius of about 8 nm and a force constant of about 400 N m^{-1} (NSC15/Al BS, Bruker). The sensitivity coefficient of all the applied AFM tips was determined by the thermal tuning method.

Before fabricating scratches and characterizing the surface morphology, it is essential to confirm the surface conditions, including the surface roughness. The applied ribbon samples in this work exhibit an atomic-scale roughness as seen in Figure S6, satisfying the experimental requirements with ultra-low surface roughness. All of the AFM measurements were conducted in the ultra-clean room condition with the temperature of (23 ± 1)°C.

To avoid surface crystallization during isothermal annealing, the ribbon samples were annealed for less than 15 min at different temperatures below T_x. As shown in Figures 1(a) and S2, the ribbon samples remain amorphous after 12-minute annealing. To eliminate contaminants and oxides on the surface of the prepared and annealed ribbon, *in situ* argon plasma cleaning was applied for 100 s. Surface diffusion coefficients were quantitatively determined by the scratch smoothing method [31,39,43]. By monitoring the evolution of scratch width during isothermal annealing, the surface diffusivity and corresponding activation energy can be deduced. To minimize the impact of bulk diffusion and shear bands, the scratch depth is restricted to 20 nm [44-47]. Isothermal annealing treatments at various temperatures were conducted in the tube-type annealing furnace under a vacuum below 5×10^{-3} Pa to prevent the possible oxidation. EDS analyses revealed no increase in surface oxygen content during annealing (Figures S7 and S8). Additional details of scratch preparation and surface diffusion coefficient estimation were given in the Supplementary Information.

2.3 Measurement of bulk relaxation dynamics

The relaxation characteristics of the as-cast ribbons were measured on a dynamic mechanical analyzer (DMA, TA, DMAQ800) in tension mode in a nitrogen-flushed atmosphere. By precisely monitoring the viscoelastic response of amorphous materials under periodic deformation, the key mechanical parameters, including storage modulus (E'), loss modulus (E''), and loss tangent ($\tan\delta = E''/E'$) were obtained. The experimental design employed a multi-frequency temperature scanning protocol, where a controlled dynamic strain of $\varepsilon = 0.01\%$ was applied under a constant heating program (from 298 to 853 K). Through the time-temperature superposition principle, this methodology effectively elucidated the dynamic characteristics of internal relaxation behavior in the material system. The activation energy spectrum for different relaxation events was characterized by measuring dynamical mechanical properties at frequencies of 0.1, 0.25, 0.5, and 1 Hz at the heating rate of 5 K min^{-1}. Simultaneously, under stress relaxation conditions where an instantaneous strain was applied at constant temperature, the temporal decay of stress was systematically recorded. By employing the normalized stress relaxation function described through the Kohlrausch-Williams-Watts (KWW) equation, this approach provided an effective approach to reveal the dynamic heterogeneity of amorphous systems.

3 Results and discussion

3.1 Characterization of surface diffusion dynamics for marginal glass-forming Fe-based MGs

Figure 1(a) shows a series of AFM images of the evolution of a prepared scratch on the $Fe_{73.5}Si_{13.5}B_9Cu_1Nb_3$ MG surface at the annealing temperature of 770 K for different time from 0 to 720 s. The HRTEM image in the down-right corner confirms the maintenance of amorphous structure after annealing for 720 s. To quantitatively exhibit the scratch evolution, the surface profiles corresponding to different annealing times were acquired along the linear scanning path, as marked by yellow dashed arrows in Figure 1(a). Firstly, it is obvious that all the scratch profiles under different annealing times in Figure 1(b) exhibit an asymmetric morphology, which is induced by the scratch preparation procedure. Then, by tracking the scratch profiles, one can see that the evolutions of scratch width W and depth h exhibit opposite evolution paths. With the annealing time increases, the scratch depth decreases while the width increases, indicating the surface diffusion induced smoothing. Previous research reveals that the scratch width is more reliable for analyzing the asymmetric scratch compared to the depth [39]. Herein, the surface diffusion rates for all marginal Fe-based MGs in this work were estimated based on the variations in the width of the prepared scratch.

In addition to the annealing temperature of 770 K, surface diffusion rates at two additional temperatures (731 and 783 K) were investigated to establish a correlation with temperature. The detailed evolution behaviors of the scratch widths at different annealing temperatures are plotted in Figure 1(c). According to eqs. (S1) and (S2), the surface diffusion coefficients D_S were calculated as 5.74×10^{-16} m^2 s^{-1} for 731 K, 2.84×10^{-15} m^2 s^{-1} for 770 K, and 3.53×10^{-15} m^2 s^{-1} for 783 K, respectively. The surface diffusion coefficient exhibits strong temperature dependence, suggesting that the surface diffusion for MGs is a thermally activated process. This is consistent with previous reports [30,31]. Based on eq. (S3) of Arrhenius temperature dependence of diffusivity, the activation energy of surface diffusion E_S can be evaluated from the linear relationship between $\ln D_S$ and $1000/T$. As shown in Figure 1(d), the detailed value of E_S for $Fe_{73.5}Si_{13.5}B_9Cu_1Nb_3$ MG in this temperature range was determined to be 2.78 ± 0.05 eV.

Similar to the experimental strategy in Figure 1, the surface diffusion coefficients and corresponding activation energies for $Fe_{77.5}Si_{13.5}B_9$, $Fe_{76.5}Si_{13.5}B_9Cu_1$, and $Fe_{74.5}Si_{13.5}B_9Nb_3$ MGs were also measured. The evolution of the scratch profile and corresponding surface diffusion ana-

lyses are detailed in Figures S9 and S10. The values of surface diffusion activation energy are summarized in Table 1. For comparison, reported values of E_S for Pd-based MGs are 0.93 eV ($Pd_{40}Cu_{30}Ni_{10}P_{20}$) and 0.83 eV ($Pd_{78}Cu_6Si_{16}$); for Au-based MG, E_S is about 1.67 eV [30,31]. Comparative analysis demonstrates that the marginal glass-forming Fe-based MGs in this work exhibit significantly larger E_S than those of other MG systems. A previous study has found that the activation energy for diffusion near a free surface is about half of that for bulk diffusion [48]. The observed correlation between bulk diffusion and T_g suggests that the higher T_g for Fe-based MGs means the slower bulk diffusion at the same temperature and larger activation energy of the bulk diffusion [33,34]. From this perspective, the activation energies of the surface diffusion for Fe-based MGs should be reasonably higher than those of other MGs.

To compare the surface diffusion behaviors of different glasses, Figure 2 presents the evaluated surface diffusion coefficients for both non-metallic glasses and MGs at their respective T_g. The D_S at T_g for Fe-based MGs in our work was obtained by extrapolating the Arrhenius fitting to higher temperatures, as detailed in the Supplementary Information. As illustrated in Figure 2, the D_S at T_g for Fe-based MGs ranges from 10^{-14} to 10^{-15} m^2 s^{-1}. In contrast, D_S for Pd-based MGs ranges from 10^{-16} to 10^{-18} m^2 s^{-1}; for Au-based MG, D_S is about 10^{-17} m^2 s^{-1}; for Cu-Zr MG, D_S is about 10^{-17} m^2 s^{-1}. Clearly, D_S of marginal glass-forming Fe-based MGs is 1-4 orders of magnitude larger than those of other MGs, close to some organic glass. One should note that the T_g determined by the stress relaxation method is different from the traditional DSC measurement. Herein, according to Figures S4 and S5, the heating process before the stress relaxation includes two stages: stage I (fast heating) and stage II (slow heating). We can roughly divide the temperature change during the entire heating process by the time used to get an equivalent heating rate. For $Fe_{74.5}Si_{13.5}B_9Cu_1Nb_3$ MG, the value of the equivalent heating rate is about 20 K min^{-1}, which is consistent with that in DSC testing. However, considering that the heating rate before stress relaxation is variable, the T_g values obtained by the two methods differ. Nevertheless, within the range of the maximum and minimum heating rates before stress relaxation (62, 0.64 K min^{-1}), according to previous research results [48], the difference in T_g is within a temperature range of 20 K. Within this T_g difference range, the corresponding surface diffusion rate differs by less than an order of magnitude. In our work, the diffusion rates of Fe-based MGs are about four orders of magnitude faster than those of stable MGs. Therefore, although the T_g determined by stress relaxation differs from that determined by DSC, when comparing the atomic mobility at T_g between different MG families, it does not change the experimental result that the diffusion rates of Fe-based MGs are much faster.

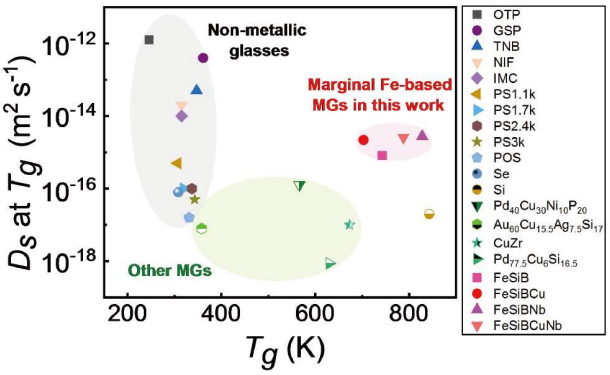

Figure 2 (Color online) Comparison of surface diffusion coefficient D_S at T_g of different glassy materials.

For MGs, the initial surface crystallization typically precedes the inner crystallization [18,31,49-51]. This phenomenon is particularly pronounced in marginal glass-forming Fe-based MGs with poor thermal stability [17,18]. The classical nucleation theory posits that surface defects, including vacancies and micropores, serve as preferential nucleation sites by effectively lowering the activation energy barrier for nucleation processes [52,53]. This fundamental mechanism explains the observed phenomenon of surface-dominated nucleation in some glasses. In the context of marginal glass systems, surface atoms exhibit enhanced diffusion kinetics due to reduced atomic constraints, enabling spontaneous structural rearrangement that facilitates critical nucleus formation. Furthermore, this dynamic atomic rearrangement establishes a self-reinforcing mechanism whereby nascent nuclei progressively evolve into stable crystalline domains through continuous surface atom ordering. Thus, the obvious surface crystallization in marginal glass-forming Fe-based MGs should be closely related to this ultrafast surface diffusion, which will be investigated in future work.

3.2 Determination of bulk relaxation spectra for marginal Fe-based MGs

Previous studies demonstrated that the surface diffusion in glasses exhibits a strong correlation with bulk fragility [32,34]. Specifically, glasses with varying fragilities exhibit distinct relaxation behaviors. It has been reported that surface diffusion in certain MGs is closely related to the typical faster relaxations within the bulk sample, such as the Johari-Goldstein β relaxation [25,33]. To investigate the correlation between surface diffusion and bulk relaxation behaviors in the marginal glass-forming Fe-based MGs, a series of DMA tests under different applied frequencies were conducted. The loss modulus E'' as a function of temperature at frequencies of 0.1, 0.25, 0.5, and 1 Hz for four marginal glass-forming Fe-based MGs are displayed in Figures 3(a), (b), and

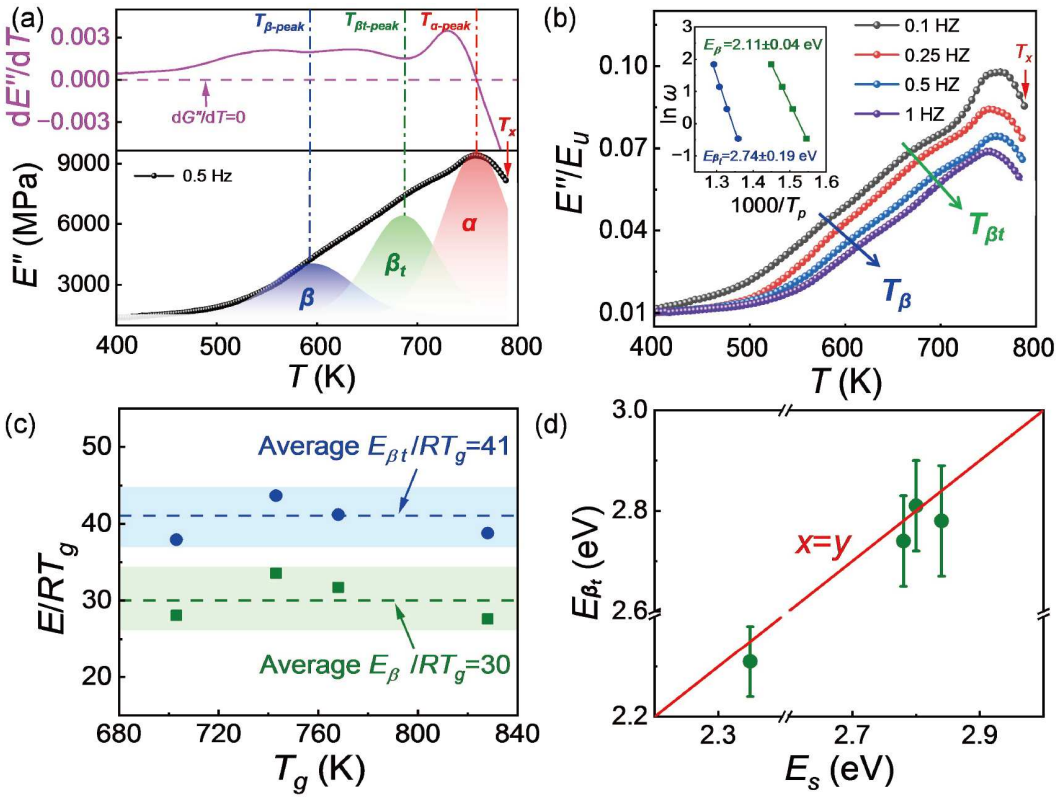

Figure 3 (Color online) Relaxation behavior of the marginal Fe-based MG system. (a) Loss modulus E'' spectrum of $Fe_{73.5}Si_{13.5}B_9Cu_1Nb_3$ MG at 0.5 Hz. The loss modulus spectrum is fitted by three different relaxation peaks, named as α, β_t, and β relaxations. The upper magenta curve shows the plot of the derivation of loss modulus and temperature. The red arrow corresponding to the T_x is drawn. (b) Reduced loss modulus spectra E''/E_u (E_u is the loss modulus at room temperature) of $Fe_{73.5}Si_{13.5}B_9Cu_1Nb_3$ MG with testing frequencies of 0.1, 0.25, 0.5, 1 Hz where E_u is the loss modulus at room temperature. The blue and green arrows give the evolution of the β and β_t relaxation peaks. The inserted plot shows the activation energies of the β and β_t relaxations. The red arrow corresponding to the T_x is also drawn. (c) Plot of E/RT_g and T_g for marginal Fe-based MGs in this work. The blue and green dashed lines give the average values of E/RT_g for the β_t and β relaxations. (d) Comparison of surface diffusion activation energy E_S and β_t relaxation activation energy $E_{\beta t}$ for four marginal Fe-based MGs. The red line gives the linear fitting equation of $x = y$.

S11, respectively. As shown in Figure 3(a), for $Fe_{73.5}Si_{13.5}B_9Cu_1Nb_3$ MG at 0.5 Hz, two distinct excess relaxation wings (β, β_t) are observed before the primary α relaxation according to the E''-T curve. In dynamic mechanical analysis of stress relaxation spectra, fitting of relaxation mode typically requires multiple mathematical models, such as the Havriliak-Negami function, the Kohlrausch-Williams-Watts equation [36]. Herein, we simply performed the profile fitting of the loss relaxation spectrum to guide the location of different relaxation modes by multiple Gaussian functions, as shown in the bottom part of Figure 3(a). Meanwhile, to clearly identify the peak temperature value corresponding to different relaxation modes, the corresponding curve of dE''/dT was also displayed in the upper part of Figure 3(a). Obviously, for $Fe_{73.5}Si_{13.5}B_9Cu_1Nb_3$ MG at 0.5 Hz, there appear three different relaxation modes. It should be noted that only the primary α relaxation displays the peak-like shape corresponding to $dE''/dT = 0$. For the other two relaxation modes with excess wing character, only the minimum values appear within the dE''/dT curve. To verify if the observed β_t relaxation comes from structural relaxation during the heating process, the as-cast samples were annealed for 10 min at the peak temperature of β_t relaxation. The corresponding DMA scan curve is shown in Figure S11. Clearly, the β_t relaxation peak is still present after annealing and remains stable in the relaxed samples. This result directly rules out the possibility of a structural relaxation effect during the heating process.

Furthermore, the corresponding reduced loss modulus spectra E''/E_u (E_u is the loss modulus at room temperature) with temperature under the frequency of 0.1, 0.25, 0.5, and 1 Hz are measured and displayed in Figure 3(b). Previous research reported that the relaxations before α relaxation feature as fast relaxation modes, which are easily activated by thermal and mechanical stimuli [36-38,54-56]. From Figure 3(b), with the applied frequency increasing, these two excess wings shift towards higher temperature, indicating their thermal activation character. To quantify the activation energy of these excess wing relaxations, the Arrhenius equation, $\ln w = \ln w_0 - E/kT$ ($w = 2\pi f$, f is the frequency) was

employed [56]. The peak temperature T_p can be obtained from the partial differential curve of the loss spectrum, as shown in the inset of Figure 3(a). The detailed calculations of E_β and $E_{\beta t}$ are inserted in Figure 3(b). Obviously, the first excess wing relaxation at a lower temperature exhibits a lower activation energy compared to the second excess wing relaxation. Similarly, the activation energies of the excess wing relaxations for the other three Fe-based MGs are determined (Figure S12) and summarized in Table 1.

One should note that the heating rate is very important for the determination of the relaxation spectrum for the glass. In our work, the heating rates during DMA measurements are 5 K min^{-1}. Compared to the heating rate of DSC measurements (20 K min^{-1}), these two heating rates are basically in the same order of magnitude, so the corresponding thermodynamic parameters, such as T_x and T_g, will not differ much. When the T_x for all Fe-based MGs in our work are drawn in Figures 3(a), (b), and S12, it is interesting to find that the onset of T_x coincides with the termination of the α relaxation. Thus, the α peaks shown in the loss modulus spectrum are not the complete α relaxation peak but only a part of the α relaxation.

Before the primary α relaxation, there are several fast relaxation modes, such as Johari-Goldstein β relaxation, fast β or γ relaxation in MGs [36]. The corresponding activation energy for the traditional Johari-Goldstein β relaxation in MGs is usually estimated using the empirical relationship $E_\beta = (26 \pm 4)RT_g$ [57]. To clarify if the two excess wing relaxations observed in this work are Johari-Goldstein β relaxation, Figure 3(c) plots E/RT_g against T_g. The average E/RT_g for the first excess wing relaxation at the lower temperature is about 30, which is close to that of Johari-Goldstein β relaxation. In contrast, the average E/RT_g for the second excess wing relaxation at the higher temperature is about 41, significantly exceeding that of Johari-Goldstein β relaxation. Thus, two excess wing relaxations observed in marginal Fe-based MGs are named as β and β_t relaxations, as shown in Figure 3(a), respectively. β_t relaxation represents an abnormal and transitional relaxation mode that existed in marginal glass-forming Fe-based MGs.

Recently, Sun et al. [37] found an anomalous relaxation α_2 in the marginal Al-Sm MG. This α_2 relaxation is located at the temperature regime between α and β relaxations, related to the transition from coupling to decoupling of Al and Sm atomic motion. When the temperature crosses the α_2 relaxation peak, the motion of Al and Sm atoms decouples. The decoupling of fast and slow motions constitutes the fundamental mechanism underlying structural non-equilibrium freezing during the glass transition process. It should be noted that, although both α_2 relaxation and β_t relaxation are located between α and β relaxation, β_t relaxation follows the Arrhenius equation with the temperature [58]. It means β_t relaxation should be governed by the collective motion of larger sizes and clusters, similar to the string-like cooperative motion of β relaxation. In contrast, α_2 relaxation follows the similar relaxation behaviors of α relaxation, which should be the macroscopic flow behavior. Thus, these two relaxation modes are significantly different and the β_t relaxation is an abnormal and unique relaxation mode in marginal glass-forming Fe-based MGs.

3.3 Correlation between surface diffusion dynamics and bulk relaxation dynamics

Previous research reported that surface diffusion is controlled by bulk fragility for various glasses, and stronger liquids have greater resistance to dynamic excitation from bulk to surface [32]. It means that there should be a close relationship between the surface diffusion dynamics and bulk relaxation dynamics. To clarify their relationship, we specially compared the activation energies of surface diffusion and the β_t relaxations for the marginal glass-forming Fe-based MGs in Figure 3(d). Before this, we have noticed that the activation energies for surface diffusion are much larger than those of β relaxations. Surprisingly, nearly one-to-one correspondence is observed between E_S and $E_{\beta t}$ rather than E_β, as marked by the red line in Figure 3(d). The above result directly demonstrates that the surface diffusion for marginal glass-forming Fe-based MGs is governed by the diffusion mode similar to the abnormal bulk β_t relaxation.

Ngai et al. [59] observed that surface diffusion coefficients remain comparable across diverse glass systems despite significant variations in structural α-relaxation dynamics. They attributed this phenomenon to the dominant role of Johari-Goldstein β-relaxation, proposing that intermolecular coupling or cooperative effects are eliminated during surface diffusion processes. For stable Pd-, Au-, and Zr-based MGs with good glass formation ability, the enhanced surface diffusion behaviors can be well explained according to the Johari-Goldstein β-relaxation. However, the surface diffusion mechanism we observed in marginal glass-forming Fe-based MGs appears distinct from the above stable MGs. The relaxation spectra of marginal glass-forming Fe-based MGs in this work exhibits the characteristic of double excess wings. Previous studies suggest that the excess wing in MGs originates from a partially developed β relaxation [60]. Considering that the β relaxation originates from the motion of string-like cooperative clusters while α relaxation corresponds to the macroscopic flow [36], the β_t relaxation between two relaxation modes should be associated with a new motion mode involving larger-sized and collective clusters rather than macroscopic flow. Meanwhile, the β_t relaxation's Arrhenius behavior suggests collective motion of larger structural units, analogous to the "string-like" cooperative motions proposed for β relaxation in fragile glasses [61]. During the formation of marginal glass-forming MGs, dy-

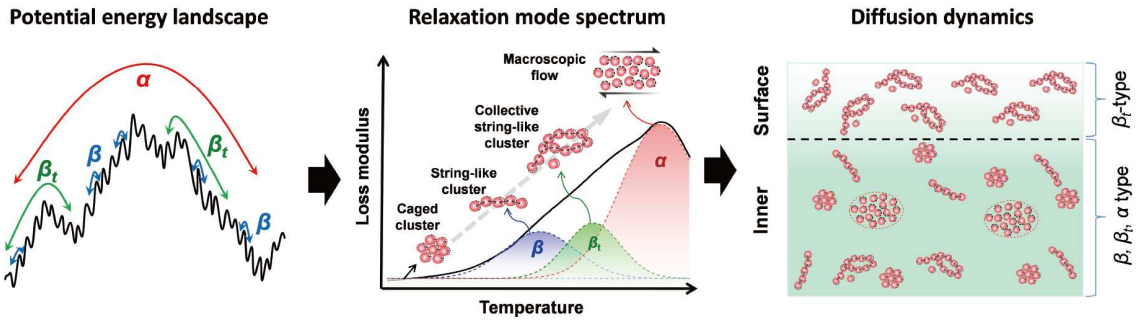

Figure 4 (Color online) One scheme of the physical mechanism of ultrafast surface diffusion in marginal Fe-based MGs from the comprehensive perspective of the potential energy landscape, the relaxation mode spectrum, and diffusion dynamics. The characteristics of the Arrhenius behavior and the larger activation energy of β_t relaxation indicate the mechanism of larger "string-like" cooperative motions.

namic activation sites with enhanced structural fluctuations emerge. These abundant sites trigger relaxation in adjacent regions, allowing dynamic promotion effects to propagate along string-like pathways. This propagative behavior drives rapid relaxation of neighboring atoms and orchestrates collective cluster motions [61,62], thereby facilitating overall diffusion. Therefore, a schematic framework was proposed to illustrate the underlying mechanism of ultrafast surface diffusion dynamics from the comprehensive view of the potential energy landscape, the relaxation mode spectrum, and diffusion dynamics, as displayed in Figure 4. In marginal Fe-based MGs, in addition to the typical α and β relaxation (red and blue curved arrows), an anomalous β_t relaxation mode with a larger activation energy than β relaxation (marked by green curved arrows) exists in both the bulk and surface. This unique relaxation mode is responsible for driving the ultrafast surface diffusion dynamics observed in marginal glass-forming Fe-based MGs. It should be noted that the above physical picture of the β_t relaxation is merely a speculation based on the current experimental results and previous research progress. To clarify the microstructural physical mechanisms of β_t relaxation, molecular dynamics simulation may be an excellent approach, which will be the focus of our next research.

The discovery of ultrafast surface diffusion dynamics governed by an abnormal β_t relaxation mode in marginal glass-forming Fe-based MGs may provide some enlightenment for deeply understanding surface dynamics and promoting surface-related applications. First, our work establishes a direct link between bulk relaxation and surface diffusion, offering transformative opportunities for practical applications of MGs by surface engineering strategy. For instance, controlling β_t relaxation enables precise tuning of surface diffusion and even surface crystallization, optimizing high-frequency soft magnetic properties by suppressing coarse-grained structures [62-65]. Second, beyond magnetism, these findings unlock new pathways for designing catalytic materials with enhanced surface reactivity, enabling cold joining in additive manufacturing, and stabilizing ultrastable glasses for advanced optical devices [23,52,58,66-68]. What is more, the identified correlation between bulk relaxation modes and surface dynamics serves as a foundational principle for tailoring functionalities across diverse fields, including energy storage, electronics, and nanotechnology. Therefore, by bridging fundamental glass physics with applied material design, this study should be helpful for starting a new era in surface-engineered MGs, where unprecedented control over surface properties drives innovation in next-generation devices.

4 Conclusion

In conclusion, we systematically studied surface diffusion dynamics and relaxation modes in four marginal glass-forming Fe-based MGs. It was found that the marginal glass-forming Fe-based MGs exhibit ultrafast surface diffusion rates, 1-4 orders of magnitude faster than those of stable MGs. For the first time, an abnormal β_t relaxation mode is identified between α and β relaxations, with activation energies matching those of surface diffusion. A cooperative cluster motion mechanism associated with β_t relaxation is proposed to explain this unprecedented surface mobility. These findings not only establish a direct correlation between bulk relaxation and surface dynamics but also bridge relaxation physics with surface engineering, providing a transformative framework for tailoring functional properties in next-generation metallic glassy materials.

This work was supported by the National Key R&D Program of China (Grant No. 2024YFB3813700), the National Natural Science Foundation of China (Grant Nos. 52471187, 52201194, 52222105, 92163108, and 52231006), 3315 Innovation Youth Talent in Ningbo City (Grant No. 2021A123G), the Zhejiang Provincial Natural Science Foundation of China (Grant No. LZY23E010002), and the Natural Science Foundation of Ningbo City (Grant No. 2023J342).

Conflict of interest The authors declare that they have no conflict of interest.

Supporting Information

The supporting information is available online at http://phys.scichina.com and https://link.springer.com. The supporting materials are published as submitted, without typesetting or editing. The responsibility for scientific accuracy and content remains entirely with the authors.

1 A. L. Greer, Science **267**, 1947 (1995).
2 M. Chen, NPG Asia Mater. **3**, 82 (2011).
3 W. H. Wang, Adv. Mater. **21**, 4524 (2009).
4 A. L. Greer, M. B. Costa, and O. S. Houghton, MRS Bull. **48**, 1054 (2023).
5 M. E. McHenry, M. A. Willard, and D. E. Laughlin, Prog. Mater. Sci. **44**, 291 (1999).
6 J. Zhou, X. Li, X. Hou, H. Ke, X. Fan, J. Luan, H. Peng, Q. Zeng, H. Lou, J. Wang, et al., Adv. Mater. **35**, 2304490 (2023).
7 H. X. Li, Z. C. Lu, S. L. Wang, Y. Wu, and Z. P. Lu, Prog. Mater. Sci. **103**, 235 (2019).
8 F. C. Li, T. Liu, J. Y. Zhang, S. Shuang, Q. Wang, A. D. Wang, J. G. Wang, and Y. Yang, Mater. Today Adv. **4**, 100027 (2019).
9 O. Gutfleisch, M. A. Willard, E. Brück, C. H. Chen, S. G. Sankar, and J. P. Liu, Adv. Mater. **23**, 821 (2011).
10 X. S. Li, J. Zhou, L. Q. Shen, B. A. Sun, H. Y. Bai, and W. H. Wang, Adv. Mater. **35**, 2205863 (2023).
11 V. Zhukova, A. Talaat, M. Ipatov, J. J. del Val, J. M. Blanco, L. Gonzalez-Legarreta, B. Hernando, R. Varga, P. Klein, M. Churyukanova, et al., J. Miner. Metals Mater. Soc. **67**, 2108 (2015).
12 X. Wang, H. J. Ma, Z. H. Sheng, S. F. Jin, W. Xu, M. Ferry, L. Chen, J. Q. Duan, and W. M. Wang, AIP Adv. **7**, 015302 (2017).
13 V. Vega, V. M. Prida, B. Hernando, M. Ipatov, A. Chizhik, V. Zhukova, A. Zhukov, L. Domínguez, and J. González, J. Mater. Res. Tech. **15**, 6929 (2021).
14 A. He, J. Li, M. Wang, A. Wang, Y. Xiao, Y. Dong, H. Guo, R. Jiang, W. Xia, L. Dong, et al., J. Mater. Sci. Tech. **120**, 1 (2022).
15 W. Zhang, R. Li, J. Wang, T. Zhang, Y. Gao, and T. Zhang, Mater. Des. **246**, 113311 (2024).
16 C. C. Yuan, F. Yang, F. Kargl, D. Holland-Moritz, M. Z. Li, X. L. Wang, B. Zhang, W. H. Wang, and A. Meyer, Acta Mater. **285**, 120652 (2025).
17 G. Herzer, and H. R. Hilzinger, Phys. Scr. **39**, 639 (1989).
18 U. Köster, Mater. Sci. Eng. **97**, 233 (1988).
19 Z. Y. Zhou, Q. Yang, and H. B. Yu, Prog. Mater. Sci. **145**, 101311 (2024).
20 H. B. Yu, L. Gao, J. Q. Gao, and K. Samwer, Natl. Sci. Rev. **11**, nwae091 (2024).
21 L. Gao, H. B. Yu, T. B. Schrøder, and J. C. Dyre, Nat. Phys. **21**, 471 (2025).
22 R. Garcia, C. J. Gómez, N. F. Martinez, S. Patil, C. Dietz, and R. Magerle, Phys. Rev. Lett. **97**, 016103 (2006).
23 J. Ma, C. Yang, X. Liu, B. Shang, Q. He, F. Li, T. Wang, D. Wei, X. Liang, X. Wu, et al., Sci. Adv. **5**, eaax7256 (2019).
24 C. R. Cao, Y. M. Lu, H. Y. Bai, and W. H. Wang, Appl. Phys. Lett. **107**, 141606 (2015).
25 K. L. Ngai, L. M. Wang, and H. B. Yu, J. Phys. Chem. Lett. **8**, 2739 (2017).
26 B. J. Gurmessa, and A. B. Croll, Phys. Rev. Lett. **110**, 074301 (2013).
27 Z. Fakhraai, and J. A. Forrest, Science **319**, 600 (2008).
28 L. Wang, A. J. G. Ellison, and D. G. Ast, J. Appl. Phys. **101**, 023530 (2007).
29 L. Zhu, C. W. Brian, S. F. Swallen, P. T. Straus, M. D. Ediger, and L. Yu, Phys. Rev. Lett. **106**, 256103 (2011).
30 C. R. Cao, L. Yu, and J. H. Perepezko, Appl. Phys. Lett. **116**, 231601 (2020).
31 Z. Wang, and J. H. Perepezko, Appl. Phys. Lett. **124**, 091601 (2024).
32 Y. Li, A. Annamareddy, D. Morgan, Z. Yu, B. Wang, C. Cao, J. H. Perepezko, M. D. Ediger, P. M. Voyles, and L. Yu, Phys. Rev. Lett. **128**, 075501 (2022).
33 A. Annamareddy, P. M. Voyles, J. Perepezko, and D. Morgan, Acta Mater. **209**, 116794 (2021).
34 A. Annamareddy, Y. Li, L. Yu, P. M. Voyles, and D. Morgan, J. Chem. Phys. **154**, 104502 (2021).
35 F. H. Stillinger, and P. G. Debenedetti, J. Chem. Phys. **116**, 3353 (2002).
36 H. B. Yu, W. H. Wang, and K. Samwer, Mater. Today **16**, 183 (2013).
37 Y. Sun, S. X. Peng, Q. Yang, F. Zhang, M. H. Yang, C. Z. Wang, K. M. Ho, and H. B. Yu, Phys. Rev. Lett. **123**, 105701 (2019).
38 R. J. Xue, L. Z. Zhao, B. Zhang, H. Y. Bai, W. H. Wang, and M. X. Pan, Appl. Phys. Lett. **107**, 241902 (2015).
39 L. Gao, Y. Sun, and H. B. Yu, Phys. Rev. B **108**, 014201 (2023).
40 R. Ishikawa, T. Futazuka, Y. Jimbo, K. Kawahara, N. Shibata, and Y. Ikuhara, Sci. Adv. **10**, eadk6501 (2024).
41 B. S. Swartzentruber, Phys. Rev. Lett. **76**, 459 (1996).
42 T. T. Tsong, Mater. Sci. Eng.-A **353**, 1 (2003).
43 E. E. Gruber, and W. W. Mullins, Acta Metall. **14**, 397 (1966).
44 R. T. King, and W. W. Mullins, Acta Metall. **10**, 601 (1962).
45 J. Dong, Y. Huan, B. Huang, J. Yi, Y. H. Liu, B. A. Sun, W. H. Wang, and H. Y. Bai, Innovation **2**, 100106 (2021).
46 M. Q. Jiang, G. Wilde, and L. H. Dai, Scripta Mater. **127**, 54 (2017).
47 C. Liu, V. Roddatis, P. Kenesei, and R. Maaß, Acta Mater. **140**, 206 (2017).
48 J. D. Stevenson, and P. G. Wolynes, J. Chem. Phys. **129**, 234514 (2008).
49 Z. Wei, C. Wang, L. Zhang, J. Luo, Y. Gao, and B. Zhao, J. Mater. Res. **39**, 1717 (2024).
50 O. G. Shpyrko, R. Streitel, V. S. K. Balagurusamy, A. Y. Grigoriev, M. Deutsch, B. M. Ocko, M. Meron, B. Lin, and P. S. Pershan, Science **313**, 77 (2006).
51 L. Chen, C. R. Cao, J. A. Shi, Z. Lu, Y. T. Sun, P. Luo, L. Gu, H. Y. Bai, M. X. Pan, and W. H. Wang, Phys. Rev. Lett. **118**, 016101 (2017).
52 K. J. Wu, E. C. M. Tse, C. Shang, and Z. Guo, Prog. Mater. Sci. **123**, 100821 (2022).
53 B. Cantor, I. T. H. Chang, P. Knight, and A. J. B. Vincent, Mater. Sci. Eng.-A **375-377**, 213 (2004).
54 L. Shao, L. Xue, J. Qiao, Q. Wang, Q. Wang, and B. Shen, Scripta Mater. **222**, 115017 (2023).
55 Y. Yang, J. Geng, Y. Cao, L. Fan, and B. Shi, Scripta Mater. **256**, 116418 (2025).
56 B. Wang, X. Q. Gao, and J. C. Qiao, Rare Metal. Mat. Eng. **53**, 70 (2024).
57 H. B. Yu, W. H. Wang, H. Y. Bai, Y. Wu, and M. W. Chen, Phys. Rev. B **81**, 220201 (2010).
58 X. Xia, S. Xie, M. Liu, H. C. Peng, N. Lu, J. Wang, M. J. Kim, and Y. Xia, Proc. Natl. Acad. Sci. USA. **110**, 6669 (2013).
59 K. L. Ngai, M. Paluch, and C. Rodríguez-Tinoco, Phys. Chem. Chem. Phys. **19**, 29905 (2017).
60 H. B. Yu, M. H. Yang, Y. Sun, F. Zhang, J. B. Liu, C. Z. Wang, K. M. Ho, R. Richert, and K. Samwer, J. Phys. Chem. Lett. **9**, 5877 (2018).
61 A. S. Keys, L. O. Hedges, J. P. Garrahan, S. C. Glotzer, and D. Chandler, Phys. Rev. X **1**, 021013 (2011).
62 Z. Hao, A. Ghanekarade, N. Zhu, K. Randazzo, D. Kawaguchi, K. Tanaka, X. Wang, D. S. Simmons, R. D. Priestley, and B. Zuo, Nature **596**, 372 (2021).
63 E. Lopatina, I. Soldatov, V. Budinsky, M. Marsilius, L. Schultz, G. Herzer, and R. Schäfer, Acta Mater. **96**, 10 (2015).
64 G. Herzer, and H. R. Hilzinger, J. Magn. Magn. Mater. **62**, 143 (1986).
65 B. Butvinová, P. Butvin, K. Brzózka, M. Kuzminski, I. Maťko, P. Švec Sr, and M. Chromčíková, J. Magn. Magn. Mater. **424**, 233 (2017).
66 O. Kovalenko, C. Brandl, L. Klinger, and E. Rabkin, Adv. Sci. **4**, 1700159 (2017).
67 Y. Qian, C. Pei, H. Ke, X. Wei, D. Wang, Y. Jia, B. Sun, G. Wang, and W. Wang, Sci. China-Phys. Mech. Astron. **68**, 246111 (2025).
68 B. Zang, L. Song, R. Parsons, J. Shen, M. Gao, Y. Zhang, J. Huo, Y. Sun, F. Li, K. Suzuki, et al., Sci. China-Phys. Mech. Astron. **66**, 256111 (2023).